Available online at www.sciencedirect.com
ScienceDirect
Thin Solid Films 516 (2008) 7125–7134
thin solid films
www.elsevier.com/locate/tsf

Research in solar cell technologies at Tallinn University of Technology

E. Mellikov *, M. Altosaar, M. Krunks, J. Krustok, T. Varema, O. Volobujeva, M. Grossberg, L. Kaupmees, T. Dedova, K. Timmo, K. Ernits, J. Kois, I. Oja Acik, M. Danilson, S. Bereznev

Tallinn University of Technology (TUT), Department of Materials Science, Ehitajate tee 5, Tallinn 19086, Estonia

Available online 23 December 2007

Abstract

The paper summarizes the results of R/D in new alternative materials and in thin film and monograin solar cells at EU Centre of Excellence in PV Materials and Devices at TUT. The defect structure of various chalcopyrite compounds ($CuInSe_2$, $CuInS_2$, $CuGaSe_2$, $CuGaTe_2$, $AgGaTe_2$, $CuInTe_2$, $AgInTe_2$, $Cu_2ZnSnSe_4$) was studied. A novel route of spray deposition was developed to prepare ZnO layers comprising nanorods as a promising material for solar cells. Technological conditions for controlled ZnS chemical bath deposition were determined. The influence of parameters of electrodeposition and annealings in different atmosphere to the composition and morphology of $CuInSe_2$ thin films was studied. Hybrid solar cells on the basis of $CuInS_2$ and CdTe photoabsorbers in combination with organic functional layers were prepared and investigated. All the obtained results were used to optimize the technology of producing solar cell structures in different designs.

Keywords: CIS; Chemical technologies; Thin films; Powders

1. Introduction

CIS and oxide materials have distinct advantages created by several technical parameters and applications. These materials are very easy to produce in thin and thick film and nanocrystalline structures [1]. Their high adsorption coefficient allows the use of very thin films and powder layers in solar cells. Near 19% conversion efficiencies have received for lab-scale $CuInSe_2$ (CIS)-based thin film solar cells [2].

The properties of different polycrystalline thin film and powder oxide and chalcopyrite (CIS) materials have been investigated at Tallinn University of Technology during the recent years. In this research we have made efforts to obtain a perfect association of our chemical knowledge in material science with physical knowledge of important electronic processes to develop new cheaper technologies and materials for solar cells.

2. Research in alternative adsorber materials

2.1. Photoluminescence

Photoluminescence (PL) is an easy-to-use and sensitive probe of defect levels inside the forbidden band. In recent years we have studied excitonic emission in $CuInS_2$, including also a very deep emission related to the isoelectronic defects [3,4]. The edge emission resulting from highly doped ternaries has been studied experimentally and theoretically in $AgGaTe_2$ [5], $CuGaTe_2$ [6], $AgInTe_2$ [7], $CuInTe_2$ [8], and in other ternaries. The ordered defect compounds (ODC) have also attracted considerable interest not only because of their potential role in high-efficiency photovoltaic devices, but also as regards the understanding of structural properties of chalcopyrite ternary compounds. We have showed that, for example, in $CuGa_3Se_5$ the shape and properties of edge emission band assure the presence of potential and compositional fluctuations. The influence of both fluctuations on the PL properties of $CuGa_3Se_5$ has been studied and the radiative recombination processes have been explained in [9]. The edge emission in $CuGaTe_2$ has been covered in [10]. In $CuGaTe_2$ (CGT) very high concentration of holes is typically seen and therefore a screening of potential fluctuations by free holes

* Corresponding author.
E-mail address: enn@edu.ttu.ee (E. Mellikov).

0040-6090/$ - see front matter © 2007 Elsevier B.V. All rights reserved.
doi:10.1016/j.tsf.2007.12.111

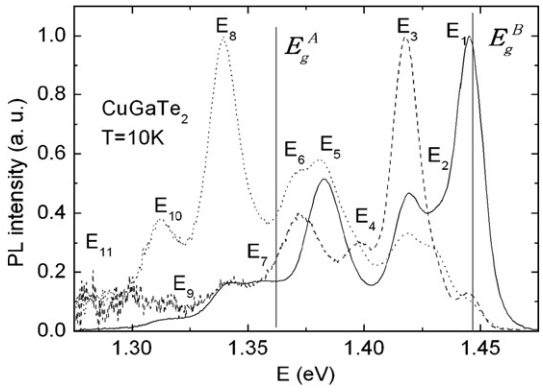

Fig. 1. PL spectra of three different samples of $CuGaTe_2$ measured at 10 K. The positions of A and B band gaps are also given as vertical lines [8].

occurs. It has been shown that the hole gas in CGT is degenerated at hole concentrations above 5×10^{18} cm^{-3}, therefore, due to Burstein–Moss shift, also different E_g values can be measured using optical absorption. Due to the screening of potential fluctuations, the edge emission of $CuGaTe_2$ has a more complex nature. The most exciting feature of the edge emission of this compound is that some PL bands are located at higher energy than the band gap energy measured by optical absorption, see Fig. 1.

It has been shown that different samples show slightly different spectra. At the same time it has been possible to detect 11 different PL bands and the peak positions of these bands in different samples seem to be the same. At least 6 PL bands had peak positions at higher energy than the lowest bandgap of CGT. The big number of discovered PL bands could be explained by resonance acceptor states (Fano-type resonances) in the upper valence band of $CuGaTe_2$, see Fig. 2.

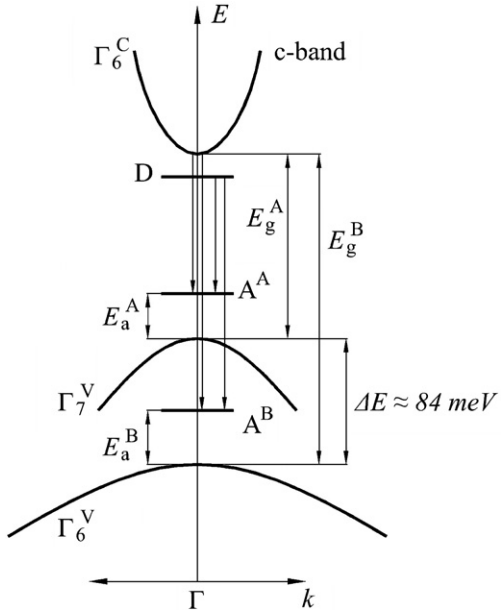

Fig. 2. A simplified figure showing the edge emission model for $CuGaTe_2$. With only one acceptor (A) and one donor (D) defect we expect 4 different PL bands to be present. Two of them are at higher energy than the lowest bandgap energy (E_g^A) and are related to the acceptor resonance state within the highest valence band [8].

2.2. Raman studies

We have performed compositional dependent Raman studies on chalcopyrite semiconductor $CuGaSe_2$ in order to study the disorder effects on the lattice vibrations. The room temperature micro-Raman spectra were recorded using a Horiba`s LabRam HR high resolution spectrometer equipped with a multichannel detection system in the backscattering configuration. The incident laser light with the wavelength of 532 nm was focused on the sample within a spot of 1 μm in diameter and the spectral resolution of the spectrometer was about 0.5 cm^{-1}.

The phase transition from $CuGaSe_2$ to ordered defect compounds (ODCs) $CuGa_3Se_5$ and $CuGa_5Se_8$ was detected (Fig. 3). The increase of structural disorder with the decrease of the [Cu]/[Ga] ratio was observed.

The chalcopyrite crystal $A^IB^{III}C_2^{VI}$, with space group $I\bar{4}2d$ and point group D^{12}_{2D}, has eight atoms per primitive cell. Its vibrational spectrum consists of 22 zone-center Raman active

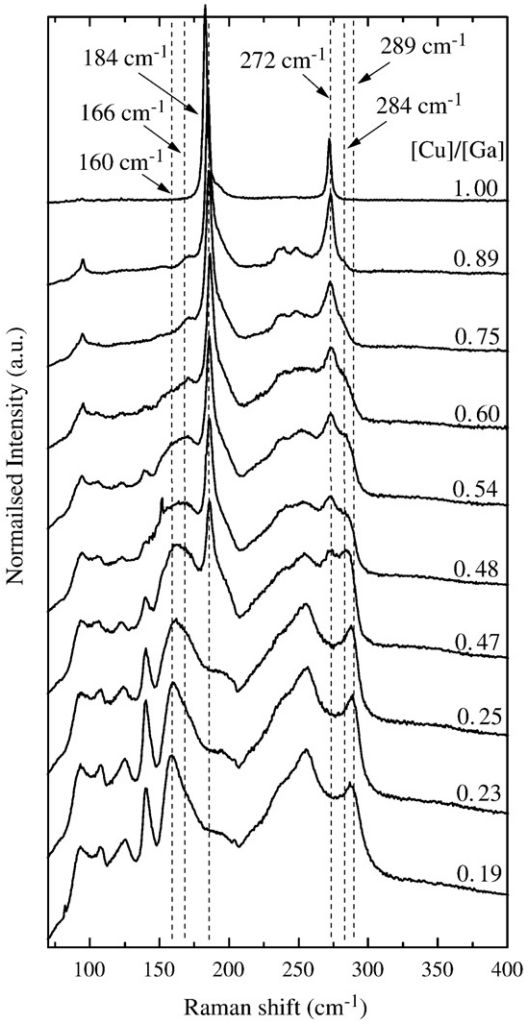

Fig. 3. Raman spectra of $Cu_xGa_ySe_2$ thin films with different [Cu]/[Ga] ratios. The Raman peaks at 272 cm^{-1}, 284 cm^{-1} and 289 cm^{-1} correspond to $B_2^1+E^5$ modes of $CuGaSe_2$, $CuGa_3Se_5$ and $CuGa_5Se_8$, respectively. The Raman peaks at 160 cm^{-1}, 166 cm^{-1} and 185 cm^{-1} correspond to A_1 mode of $CuGaSe_2$, $CuGa_3Se_5$ and $CuGa_5Se_8$, respectively.

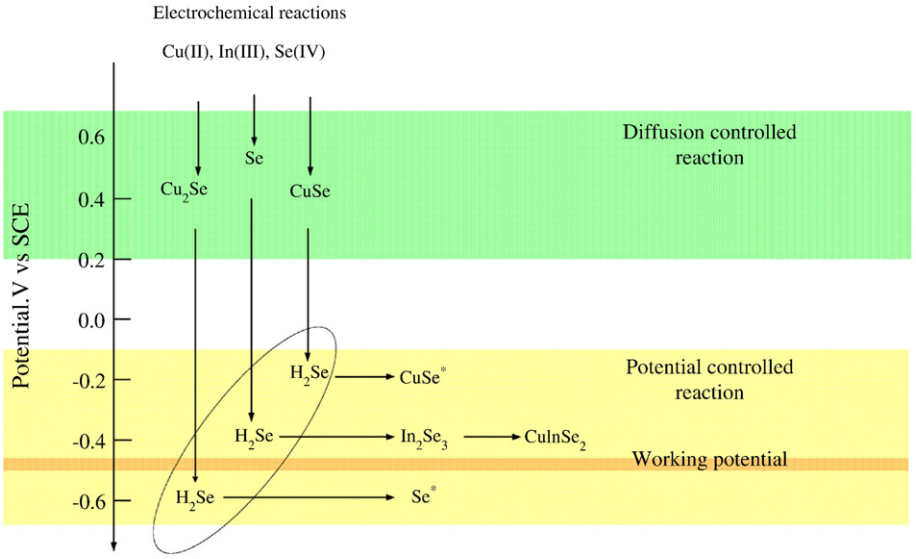

Fig. 4. Simplified scheme showing the mechanism of compound formation at the electrochemical deposition of $CuInSe_2$.

vibrational modes: $1A_1+3B_1+3B_2(LO)+3B_2(TO)+6E(LO)+6E(TO)$, from which the A_1 mode that has been ascribed to the motion of Se atom relative to Cu and Ga atoms at rest is usually dominating the Raman spectra. The spectral position of these modes depends on the defect concentration and deviation from stoichiometry. Since both the normal chalcopyrites and OVC compounds belong to the same space group, it is expected that their vibrational spectra are also very similar. Due to the presence of the vacancy in the ODC the stretching forces between nearest neighbor atoms are relaxed, thus reducing the corresponding vibrational frequencies compared to normal chalcopyrites. The recorded A_1 mode frequencies of normal chalcopyrite $CuGaSe_2$ and ODCs are in very good agreement with the theoretically expected values [11]. Apart from the frequency, also the full width at half maximum of the A_1 Raman mode is broadening with the increase of Ga content. Differences in the degree of disorder and the defect concentration may be responsible for the observed changes in Raman mode width as a function of the [Cu]/[Ga] ratio and the process of growth.

3. Electrodeposition of $CuInSe_2$ thin films

This part summarizes our latest results of the investigation in the field of one-step electrodeposition $CuInSe_2$ thin films. The electrochemical synthesis of CISe films with a thickness of about 1 μm onto glass/ITO substrates was performed potentiostatically at a potential of −500−−900 mV vs. SCE in a standard three-electrode cell. Aqueous solutions of 10 mM selenious acid and 7–20 mM indium and 1–10 mM copper sulfates were used as precursor solutions for $CuInSe_2$ film deposition. Potassium chloride acting as a complexing agent of metallic ions was used for the electrodeposition in concentrations 0–1 mol/l. The pH of electrochemical bath was in the region of 1–3. The deposition potential varied in the range −0.5 to −0.8 V vs. SCE. All the chemicals of an analytical grade (Merck) were dissolved in 18 M Ohm cm Millipore water.

Our results indicate that the mechanism of $CuInSe_2$ phase formation in one-step electrodeposition goes through a number of consecutive reactions. The formation of Cu+Se phases precedes the assimilation of indium and $CuInSe_2$ compound formation. Under the conditions of electrodeposition all three elements in the one-step electrochemical deposition process, the formation of Cu+Se phases, are controlled by the diffusion of selenium and copper species, the insertion of indium into the film depends on the applied potential (Fig. 4). The XRD analysis of deposited films confirms the formation of CuSe and Cu_2Se phases at low potentials (0 to −0.3 V) and formation of $CuInSe_2$ and In_2Se_3 at more negative potentials (−0.4 V to −0.9 V).

The associated model was used to determine the fluxes of copper, indium and selenium species to the cathode and relative concentrations of deposited solid phases. The results of computations enable us to build the distribution diagram of the final products (Fig. 5).

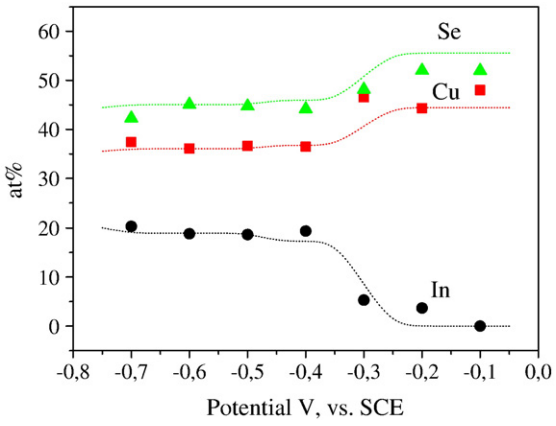

Fig. 5. Calculated (dotted lines) and the observed variation of film composition with deposition potential. Films were obtained from 10 mM $CuCl_2$, 5 mM In_2Cl_3 and 10mMSeO_2 solution, pH=2.

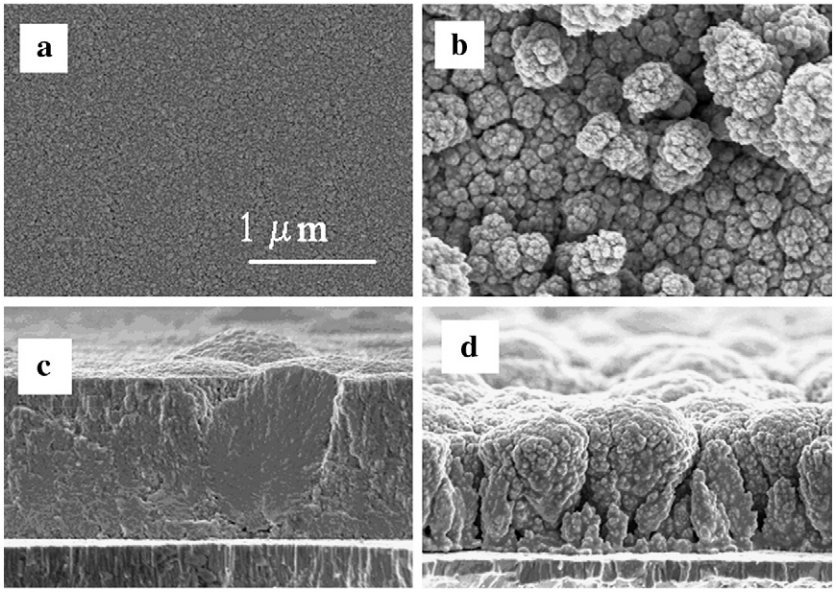

Fig. 6. Surface and cross-section images of $CuInSe_2$ thin films electrodeposited from solution 5 mM $CuSO_4$, 10 mM $In_2(SO_4)_3$ and 10 mM SeO_2 at potential −600 mV vs. SCE: a, b) diffusion of reacting species is not limited; c,d) under diffusion limitation.

Investigations of films show that the morphology of films is determined by the nucleation rate of crystals (is the function of overpotential) and the rate of mass transport of solute species. The nucleation rate of copper selenides establishes the morphology of $CuInSe_2$ at all. As the electrodeposition of $CuInSe_2$ can occur at potentials −0.4 V vs. SCE, an initial formation of copper selenides occurs under substantial overpotential (deposition potential CuSe+0.5 V vs. SCE). Dense, smooth films were obtained, when the rate of deposition was not limited by the diffusion of reacting species (Fig. 6a and b) [12]. The $CuInSe_2$ films formed under the conditions of the limiting diffusion of current density were of dendritic and porous structure (Fig. 6c and d) [13]. At the same time, the composition of films was nearly stoichiometric.

4. Electrochemical etching of $CuInSe_2$ films

The chemical etching in KCN solutions is the prevalent method to remove segregated Cu–Se and Cu–S phases from CIS films [14,15]. Another approach to modify the surface of films is an exposure of the surface to strong oxidants, such as Br [15], H_2O_2 [16], permanganates [16] or complexes [17]. We have developed two methods of the electrochemical removal of $Cu_{2-x}Se$ from the surface of $CuInSe_2$ films [18]. The first of the methods is based on cycle scanning of voltage from −0.5 V to +0.5 V in an acidic electrolyte. The other method is based on an anodic oxidation of $Cu_{2-x}Se$ at the potentiostatic regime +0.5 V in the basic solution. Both treatments yield in a selective dissolution of cuprous selenides from the film surface. Table 1 shows the composition of unetched films and of electrochemically and KCN etched films.

Changes in the microstructure of the films were studied by help of cross-sectional SEM images (Fig. 7). The initial electrodeposited and annealed in a vacuum thin $CuInSe_2$ films with thickness about 0.8 μm have a dense, uniform structure. Cross-sectional images of etched films (Fig. 7b–d) reveal a porous structure, resulting in the removal of separate phase of $Cu_{2x}Se$ in the etching process of $CuInSe_2$ films. The grain boundary cracks extending through the film were expanded. If the chemical etching of $Cu_{2x}Se$ phases in KCN solution effects only the film surface structure and composition (Fig. 7b), then electroetching removes $Cu_{2x}Se$ phases additionally from the intergrain areas leading to the formation of deep cracks through the film (Fig. 7c and d).

5. Sol–gel derived flat and porous TiO_2 films

Sol–gel derived TiO_2 films as components of DSSC and eta-cells were deposited by spray pyrolysis and spin-coating techniques. The film formation process was monitored by thermal analysis measurements. In order to find the proper temperature profile for TiO_2 film deposition, comprehensive thermal analyses (TG/DTG/DTA coupled with EGA-FTIR and MS) were conducted on dried TiO_2-gel powders [19,20]. Our studies [21,22] revealed that phase composition and crystallinity of sol–gel spray deposited TiO_2 films, grown from solution containing titanium(IV) tetraisopropoxide, acetylacetone and ethanol, are controlled by both deposition and annealing temperatures. As-deposited films grown onto silicon substrates at

Table 1
Composition of annealed and etched films

Method of etching	Cu at.%	In at.%	Se at.%
Unetched	28.6	25.0	46.4
Chemical etching (3 min) 10% KCN and 0.5% KOH	25.9	26.7	47.4
Electrochemical etching 0.1 M H_2SO_4 (pH=1.2) scanning potential −0.5–+0.5 V, scan rate 10 mV/s	25.2	25.0	49.8
Electrochemical etching 0.1 M NaOH (pH=13.2) potential +0.4 V	24.0	24.7	51.3

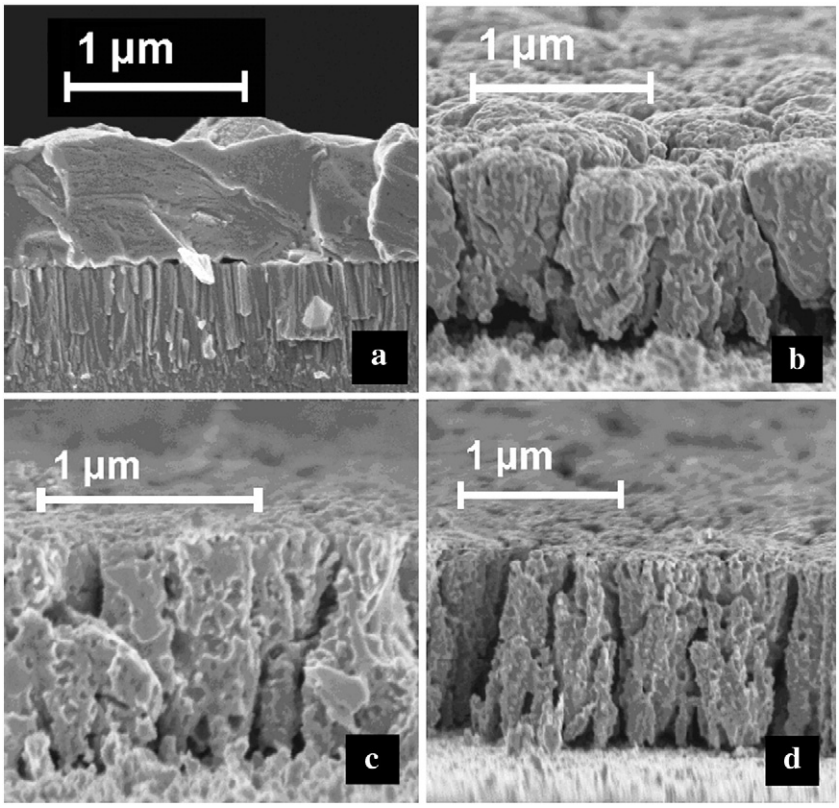

Fig. 7. SEM images ff cross-section of CISe films: unetched (a), etched in 5%KCN (b), electroetched in 0.1 M H_2SO_4 (c), electroetched in 0.1 M NaOH (d) [16].

T_S < 500 °C are amorphous but crystalline films could be obtained by deposition at 500 °C or by post-deposition annealing at 500 °C and above. According to XRD annealing at 700 and 800 °C results in a mixture of anatase and rutile or rutile if grown at T_S = 435 °C or 500 °C, respectively, whereas the films grown at T_S < 400 °C remain anatase. Sprayed TiO_2 films show surface roughness below 1 nm, refractive indices of 2.1–2.3 and 2.6 and effective dielectric constant values between 36–46 and 53–70 for the anatase and rutile phases, respectively. The obtained resistivity values for TiO_2-anatase and -rutile films were in the order of 10^6 and 10^7 Ω·cm, respectively.

In order to obtain porous TiO_2 films by the sol–gel spray pyrolysis and spin-coating techniques, polyethylene glycol 600

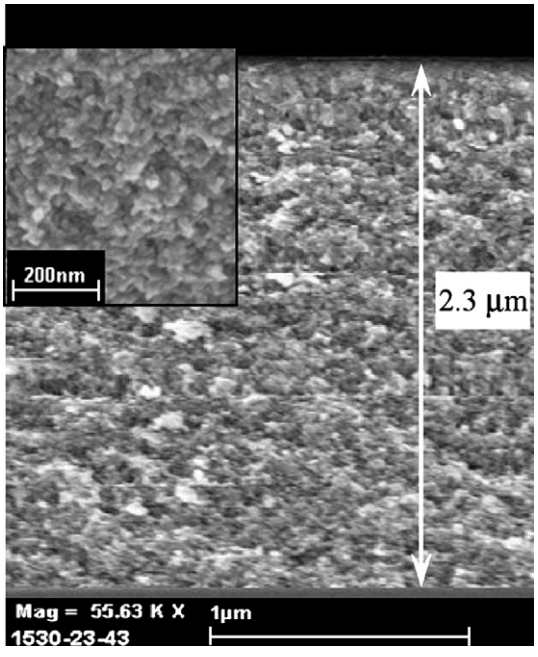

Fig. 8. SEM image of the cross-section of sprayed TiO_2 film prepared from a solution containing TTIP:PEG600 in a molar ratio of 1:7.7.

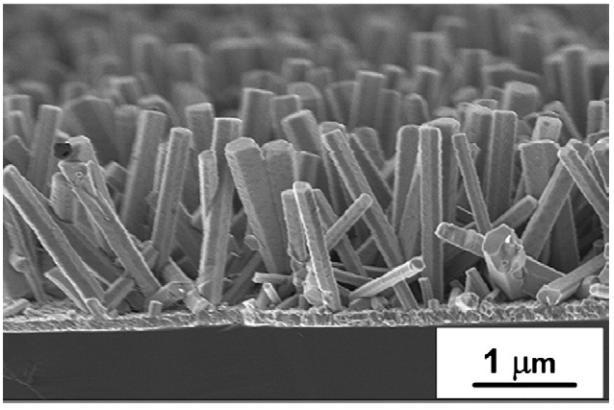

Fig. 9. SEM cross-sectional image of the ZnO layer deposited onto ITO covered glass at substrate temperature of 560 °C using zinc chloride aqueous solution with concentration of 0.1 mol/l.

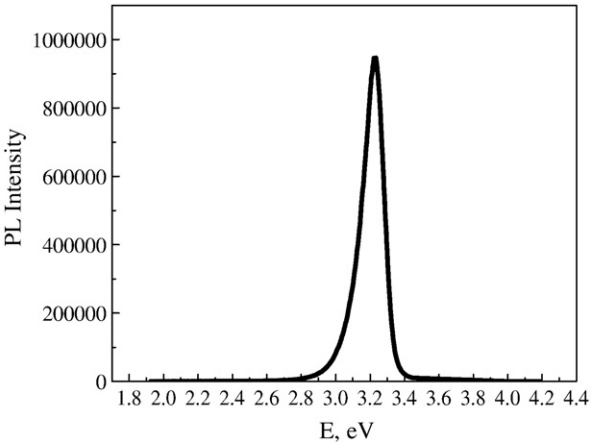

Fig. 10. Room temperature PL spectrum of ZnO nanorod layer grown by spray at 560 ° C.

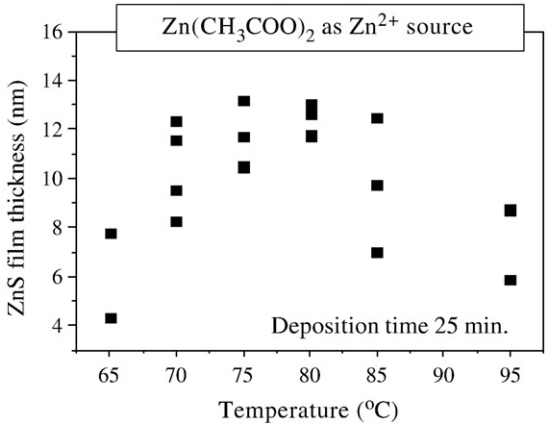

Fig. 11. Temperature dependence of ZnS deposition rate.

as a structure directing agent was added into the solution [23]. According to the results of SEM investigations, relatively well-adherent TiO_2 films with pore sizes up to 40 and 30 nm could be deposited from the used precursor solutions by spray pyrolysis and spin-coating methods, respectively. The SEM cross-sectional image of nanoporous TiO_2 film deposited by spray technique is presented in Fig. 8. Crystalline TiO_2-anatase films could be grown by spray pyrolysis at $T_S = 500$ °C, whereas in the case of spin-coating, post-deposition annealing at temperatures in the order of 700 °C is needed.

6. ZnO nanostructured layers by spray pyrolysis

It has been shown [24,25] that ZnO structured layers comprising single crystalline nanorods can be prepared by the spray pyrolysis deposition of zinc chloride aqueous solutions at temperatures 490–560 °C. The formation and shape of the rods strongly depends on the growth temperature, precursor concentration and underlayer microstructure [24,25]. ZnO nanorods with the diameter of 70–200 nm and the length of 2000 nm result in the aspect ratio up to 20. The SEM cross-sectional view of the ZnO nanorod array grown on ITO substrates is shown in Fig. 9.

Photoluminescence spectra showing strong near band edge emission around 3.36 eV at 10 K, ascribed to the exciton transition bound to neutral donors, and no emission caused by deep levels reveal that ZnO rods prepared by spray pyrolysis are of high optical and crystal quality. Room temperature PL spectrum of sprayed ZnO nanorods is presented in Fig. 10.

Table 2
ZnS chemical bath deposition on $CuInS_2$

Film	Zn source	pH	Time (min)	T, °C	Thickness (nm), by SEM	Deposition rate evaluated by the appearance of colloids
1. ZnS	$ZnSO_4$	1.7	20	70	24.3	Slow
2. ZnS	$ZnSO_4$	2.5	4	70	4.4	Very fast
3. ZnS	$ZnSO_4$	10.0	6	85	6.4	Fast
4. ZnS	$ZnSO_4$	11.0	18	85	14.1	Average
5. ZnS	$ZnSO_4$	11.5	22	85	12.3	Slow
CdS		10.3	12	90	18.5	Average
ZnSAc	Zn $(CH_3COO)_2$	11.0	25	85	9.7	Slow

7. Chemical bath deposition of ZnS on $CuInS_2$ thin films

ZnS is one of the favourable candidates to substitute CdS buffer in $CuInS_2$ solar cells. ZnS is attractive mainly because of its chemical and electrical compatibility with CIS and higher band gap energy value compared to CdS, which makes it more transparent in short wavelength region. In the present work thin-film ZnS buffer layers have been deposited at different temperatures, pH values of the solution and Zn-source onto $CuInS_2$ absorber to find optimum conditions for deposition (Table 2).

Considering films growth rate the optimal deposition temperature and pH for ZnS deposition were found to be at 80 °C and pH = 11 (Fig. 11). Layers growth rate and shape of crystals in ZnS buffer layers deposited in acidic and basic solutions are different (Table 2). Films grown in use of $ZnSO_4$ as Zn source

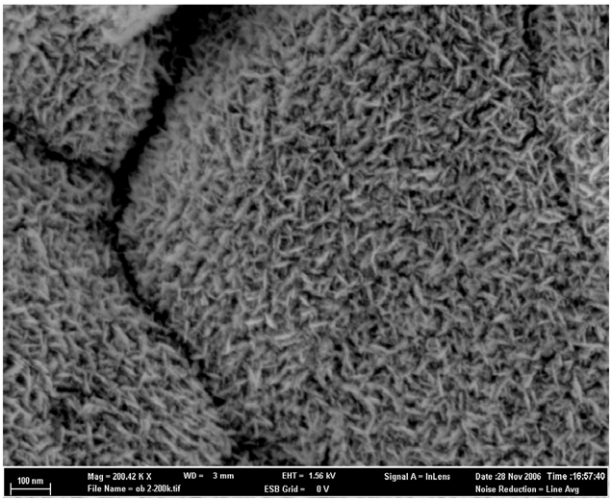

Fig. 12. SEM image of ZnS buffer layer deposited from acid bath.

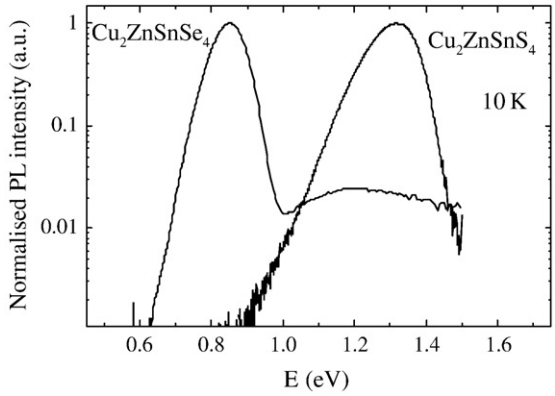

Fig. 13. Normalised PL spectra of $Cu_2ZnSnSe_4$ and Cu_2ZnSnS_4 monograin powders.

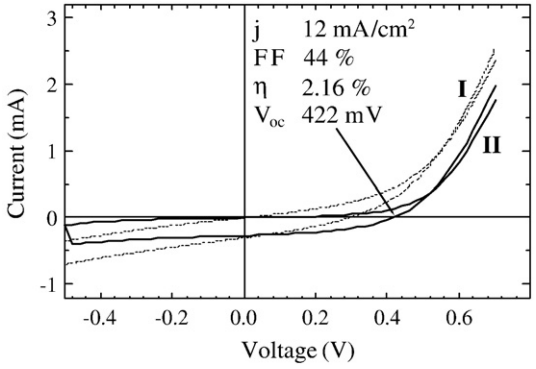

Fig. 15. IV curves of monograin layer solar cell: I — after formation, II — after 2 months.

are less dense, the use of Zn acetate as Zn source leads to denser films with bigger grains. The use of acidic solutions lead to the changes in shape of crystals (Fig. 12).

8. Solar cells with In-free adsorbers

$Cu_2ZnSnSe_4$ (CZTSe) and Cu_2ZnSnS_4 are perspective In-free adsorber materials. We synthesized $Cu_2ZnSnSe_4$ and Cu_2ZnSnS_4 powder materials from CuSe(S), ZnSe(S) and SnSe(S), CdSe(S) precursors in molten KI. More details about this process can be found elsewhere [26,27]. EDS results indicated to the homogeneous distribution of constituent elements over polished individual $Cu_2ZnCdSnSe(S)_4$ powder crystals. Composition of used materials was characterised by ratios Cu/Zn+Sn=0.85–0.9, Zn/Sn=1.04 and Se/metals=1. X-ray diffraction (XRD) measurements were performed to identify the synthesized powder material. All the appeared diffraction peaks were identified belonging to the $Cu_2ZnSnSe_4$ compound with the stannite structure (space group $I\bar{4}2m$). Any other peaks was not found [26]. PL spectra of $Cu_2ZnSnSe_4$ and Cu_2ZnSnS_4 are presented in Fig. 13. The PL spectrum of Cu_2Zn SnS_4 with the peak position at 1.31 eV is similar to that one described by K. Tanaka et al. [28]. They attributed the detected PL band between 1.1–1.45 eV to donor–acceptor pair recombination with an activation energy of 48 meV. Our measurements support qualification of band as a band-to-tail (BT) recombination band, very similar to the edge emission of other chalcopyrites [29]. The PL spectrum of $Cu_2ZnSnSe_4$ shows one nearly symmetrical band with the band maximum at 0.85 eV and very low emission around 1.2 eV. Temperature and excitation power density dependant measurements of the 0.85 eV band confirm that this PL band behaves like a band-to-tail (BT) emission in ternaries: the energy of band maximum [29].

Narrow granulometric fractions of the grown powders were used as absorber material in monogran layer (MGL) solar cell structures: graphite/CZTSe/CdS/ZnO. Powder crystals were covered with CdS thin layer by chemical bath deposition. For MGL formation a monolayer of nearly unisize grains was sedimentated into a thin layer of epoxy resin, so that the contamination of upper surfaces of crystals with epoxy was avoided. After polymerization of epoxy, ZnO window layer was deposited onto front side of MGL by RF-sputtering. Solar cell structures were completed by vacuum evaporation of 1–2 μm thick In grid contacts onto the ZnO window layer. After glueing the structures on glass substrates, the back contact area of crystals covered with epoxy was opened by etching epoxy with H_2SO_4 followed by an additional abrasive treatment. The back contact was made using graphite paste (Fig. 14). $Cu_2ZnSnSe_4$ solar cells showed the highest value of open circuit voltage V_{oc}=422 mV (Fig. 15). The temperature dependence of V_{oc} gave the barrier height of the junction F=758 meV. This value is much lower than that one possible with an absorber material with the band gap value of 1.44 eV (Fig. 16). This discrepancy could be explained as a result of formation of some narrow band gap compounds or solid solutions on the surface and this surface

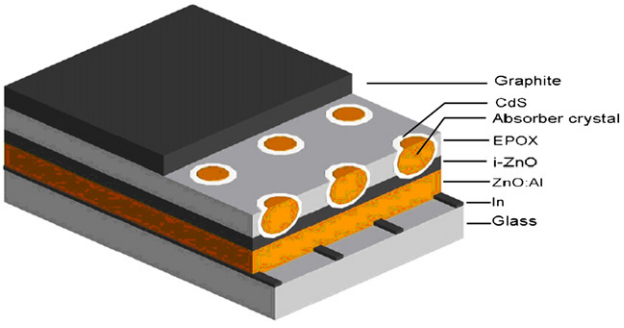

Fig. 14. Monograin layer CZTS solar cell.

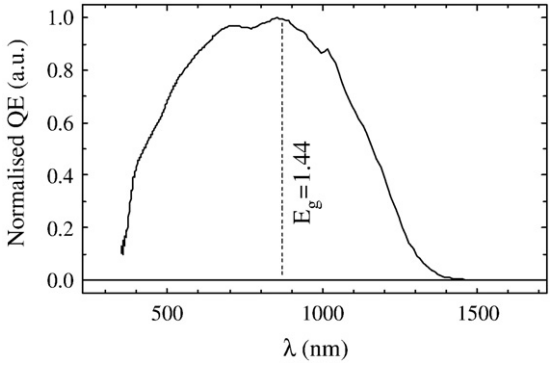

Fig. 16. Normalized spectral response curve of $Cu_2ZnSnSe_4$ solar cell.

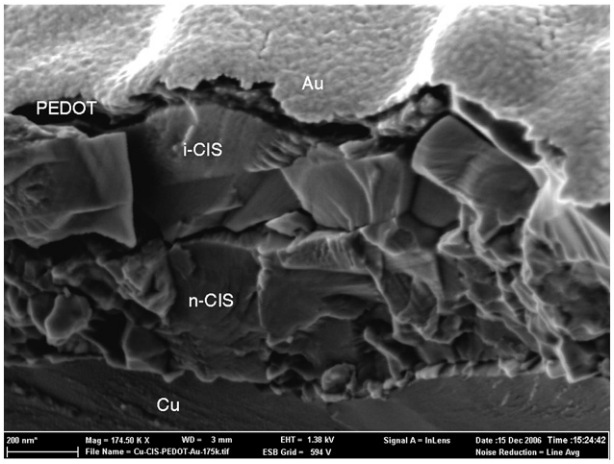

Fig. 17. Cross-sectional image of the Cu/CIS/PEDOT-PSS/Au PV structure.

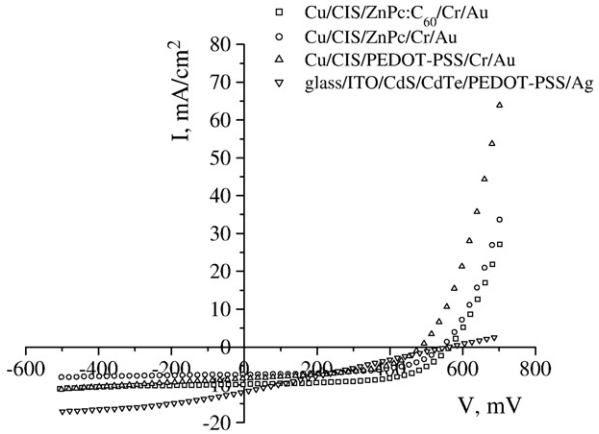

Fig. 18. Photocurrent–voltage characteristic of structures with different organic functional layers under white light illumination of 100 mW/cm^2.

layer limits the efficient work of solar cells. Further investigations are needed to clarify the origin of the PL band at 0.85 eV and to find methods to avoid the formation of the possible surface layers.

9. Solar cells with organic functional layers

Among various types of organic solar cells, the organic–inorganic hybrid structures are among the most promising types, which include flexible and inexpensive solar panels due to the potential for producing light [30]. However, the efficiency of power conversion provides advantages of organic materials as functional layers and the use of good well-known inorganic photoabsorbers (CdTe, CdSe, $CuInS_2$ etc.) [31–35]. The idea of using organic materials is supported by the fact that no dangling bonds exist on the surface of organic semiconductors and they should not create additional centres of trapping and recombination at the interface with an inorganic photoabsorber. Furthermore, the large dimensions of organic molecules should strongly limit the rate of their diffusion in inorganic layers and the formation of new impurity centres [35].

Initial Cu/CIS structures were fabricated at Institut für Solartechnologien (Frankfurt (Oder), Germany) by the so-called CISCuT deposition method [36]. A number of new hybrid solar cells based on Cu/CIS substrate/absorber and organic buffer layers of Zn-phthalocyanine (ZnPc), ZnPc:C_{60} composite, and conductive polymer buffer layer of poly(3,4-ethylenedioxythiophene) (PEDOT) doped with polystyrenesulfonate (PSS) were prepared and investigated. In this approach, the organic layer is considered by us as an alternative for the traditional buffer layer in the conventional cell structure.

All the investigated photovoltaic structures were fabricated in sandwich configurations Cu/CIS/ZnPc/Cr/Au, Cu/CIS/ZnPc:C_{60}/Cr/Au and Cu/CIS/PEDOT-PSS/Cr/Au. The spin casting and evaporation techniques were applied for organic layers deposition. Fig. 17 shows the cross-sectional image of complete structure with the PEDOT-PSS buffer layer.

The complete CISCuT structures of 2 cm^2 active areas with organic functional layers has been reported to show a photoconversion efficiency of around 3. 3% under tungsten-halogen lamp light illumination of 100 mW/cm^2 intensity [37] (see also Table 3 and Fig. 18). Also, hybrid solar cells on the basis of CdTe photoabsorber layer and CdS buffer layer on glass/ITO substrate in combination with organic back-contact layer of highly conductive PEDOT-PSS were prepared using vacuum evaporation and spin-casting techniques. Due to its high work function, CdTe is a difficult material to form an ohmic contact. When a metal contact is applied on the CdTe, this often results in the formation of a Schottky barrier. The barrier acts as a diode in the opposite direction, thus blocking the photo-generated

Table 3
PV parameters of structures with organic functional layers under white light illumination of 100 mW/cm^2

Structure	V_{oc}, mV	I_{sc}, mA/cm^2	FF	Active area S_{act}, cm^2	Efficiency η, %
Cu/CIS/ZnPc:C_{60}/Cr/Au [30]	560	9.9	0.60	2	3.3
Cu/CIS/ZnPc/Cr/Au [30]	542	7.3	0.58	2	2.3
Cu/CIS/PEDOT-PSS/Cr/Au [30]	485	8.3	0.51	2	2.1
Glass/ITO/CdS/CdTe/PEDOT-PSS/Ag	560	11.9	0.26	0.5	1.7

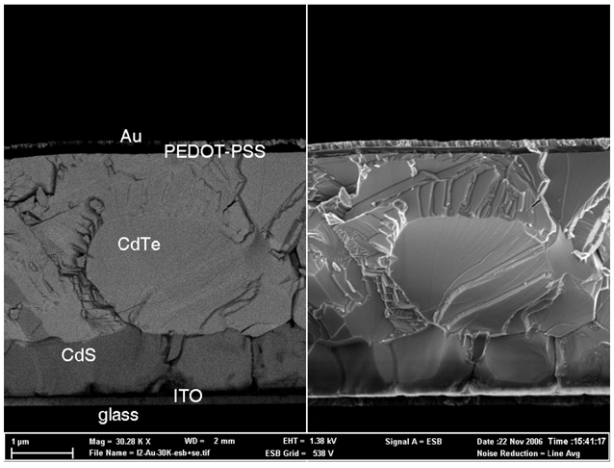

Fig. 19. Cross-sectional image of the glass/ITO/CdS/CdTe/PEDOT-PSS/Au PV structure.

charge carriers [33]. In this approach, the organic layer is considered as an alternative for the traditional back-contact layer in the conventional cell structure. For our investigations, glass/ITO/CdS/CdTe structures were used, fabricated by Dr. G. Khripunov (Thin Film Physics Group, ETH Zürich). The investigated photovoltaic structures were prepared in sandwich configurations glass/ITO/CdS/CdTe/PEDOT-PSS/Au and glass/ITO/CdS/CdTe/PEDOT-PSS/Ag. Fig. 19 shows the cross-sectional view of the complete structure with the PEDOT-PSS back-contact layer.

In order to prepare complete solar cells, the appropriate deposition parameters and thickness of highly conductive PEDOT-PSS layers were selected experimentally. The best result was obtained by spin-coating of PEDOT-PSS aqueous dispersion which was mixed with glycerin, *N*-methyl-2-pyrrolidone (NMP), isopropanol and tetraethoxysilane to enhance the electrical conductivity of the deposited PEDOT-PSS films. It was found that the prepared conductive polymer film gives good ohmic stable back-contact to the surface of the p-CdTe semiconductor film in a complete solar cell. To prepare a current contact to the PEDOT-PSS layer, the silver suspension deposition and gold evaporation techniques were applied separately. The best structure glass/ITO/CdS/CdTe/PEDOT-PSS obtained so far showed an open-circuit voltage of around 500 mV and a short-circuit current density of around 15 mA/cm^2 under white light illumination with an intensity of 100 mW/cm^2 (see also Table 3 and Fig. 18).

10. Conclusions

Our results indicate to the need for additional more detailed research in field of physical parameters of new adsorbers alternative to $CuInSe_2$ (CuInS2) materials ($CuInSe_2$, $CuInS_2$, $CuGaSe_2$, $CuGaTe_2$, $AgGaTe_2$, $CuInTe_2$, $AgInTe_2$, $Cu_2ZnSnSe_4$). Influence of different experimental parameters to the ZnS chemical bath deposition are investigated and the optimal technological parameters for ZnS deposition are determined. It was found, that the recrystallization processes during the annealing of electrodeposited $CuInSe_2$ thin films are dependent on Se vapour pressure and precursor film composition. For samples annealed in Se vapour at 450 °C, recrystallization of chalcogenide $CuInSe_2$ occurs rapidly and leads to the formation of CIS grains different by size and composition.

A novel synthesis route of spray deposition was developed to prepare ZnO layers comprising zinc oxide nanorods as a promising material for solar cells. Solar cell structures in use of In-free adsorbers are developed and bottlenecks of used technologies discussed. A new approach connected with using of organic functional layers in the solar cells structure is highlighted — hybrid solar cells based on the CIS and CdTe photoabsorber and utilizing thin film contact-buffer layers of the conductive polymer PEDOT-PSS and the organic photoabsorber ZnPc or a ZnPc:C_{60} composite were prepared and characterised.

Acknowledgements

The financial support for this research by the EU project ENK6-CT-2002-80664 (PV-EST) and by different Estonian Science Foundation grants (G6179, G6554, G6160, G6162, G6954) is gratefully acknowledged.

References

[1] A. Goetzberger, C. Hebling, H.-W. Schock, Mater. Sci. Eng. R Rep. 40 (2003) 1.
[2] M.C. Contreras, K. Ramanathan, J. AbuShama, F. Hasoon, D.L. Young, B. Egaas, R. Noufi, Prog. Photovolt. Res. Appl. 13 (7) (2005) 209.
[3] J. Krustok, J. Raudoja, R. Jaaniso, Appl. Phys. Lett. 89 (2006) 051905.
[4] M.V. Yakushev, A.V. Mudryi, I.V. Victorov, J. Krustok, E. Mellikov, Appl. Phys. Lett. 88 (No.1) (2006) 011922 (1–3).
[5] J. Krustok, A. Jagomägi, M. Grossberg, J. Raudoja, M. Danilson, Sol. Energy Mater. Sol. Cells 90 (No. 13) (2006) 1973.
[6] A. Jagomägi, J. Krustok, M. Grossberg, M. Danilson, J. Raudoja, Phys. Status Solidi (A) 203 (No. 5) (2006) 949.
[7] A. Jagomägi, J. Krustok, J. Raudoja, M. Grossberg, I. Oja, M. Krunks, M. Danilson, Thin Solid Films 480–481 (2005) 246.
[8] A. Jagomägi, J. Krustok, J. Raudoja, M. Grossberg, M. Danilson, Phys. Status Solidi (B) 237 (2) (2003) R3.
[9] M. Grossberg, J. Krustok, A. Jagomägi, M. Leon, E. Arushanov, A. Nateprov, I. Bodnar, Thin Solid Films 515 (2007) 6204.
[10] J. Krustok, M. Grossberg, A. Jagomägi, M. Danilson, J. Raudoja, Thin Solid Films 515 (2007) 6192.
[11] C. Rincon, S.M. Wasim, G. Marin, J.M. Delgado, J.R. Huntzinger, A. Zwick, J. Galibert, J. Appl. Phys. Lett. 73 (1998) 441.
[12] M.A. Contreras, K. Ramanathan, J. AbuShama, F. Hasoon, D.L. Young, B. Egaas, R. Noufi, Prog. Photovolt. Res. Appl. 13 (2005) 209.
[13] R. Gay, V. Probst, F.H. Karg, D.E. Tarrant, Proc. 3rd World Conf. Photovoltaic Energy Conversion, Osaka, Japan, 2003, p. 325.
[14] B. Canava, J.F. Guillemoles, J. Vigneron, D. Lincot, A. Etcheberry, J. Phys. Chem. Sol. 64 (2003) 1791.
[15] K. Müller, R. Scheer, Y. Burkov, D. Schmeißer, Thin Solid Films 451 (2004) 120.
[16] S. Percharmant, J.-F. Guillemoles, J. Vedel, D. Lincot, 11th Int. Conf. on Ternary and Multinary Compounds ICTMC-11 Salford, 1997, p. 719.
[17] T. Delsol, M.C. Simmonds, I.M. Dharmadasa, Sol. Energy Mater. Sol. Cells 77 (2003) 331.
[18] J. Kois, S. Bereznev, O. Volobujeva, E. Mellikov, Thin Solid Films 515 (2007) 5871.
[19] M. Krunks, I. Oja, K. Tõnsuaadu, M. Es-Souni, M. Gruselle, L. Niinistö, J. Therm. Anal. Calorim. 80 (2005) 483.
[20] I. Oja Açik, J. Madarász, M. Krunks, K. Tõnsuaadu, D. Janke, G. Pokol, L. Niinistö, J. Therm. Anal. Calorim. 88 (2007) 557.
[21] I. Oja, A. Mere, M. Krunks, C-H. Solterbeck, M. Es-Souni, Solid State Phenom. 99–100 (2004) 259.
[22] I. Oja, A. Mere, M. Krunks, R. Nisumaa, C-H. Solterbeck, M. Es-Souni, Thin Solid Films 515 (2006) 674.
[23] J. Sabataityté, I. Oja, F. Lenzmann, O. Volobujeva, M. Krunks, Comptes Rendus Chimie 9 (2006) 708.
[24] M. Krunks, T. Dedova, I. Oja, Thin Solid Films 515 (2006) 1157.
[25] T. Dedova, M. Krunks, A. Mere, J. Klauson, O. Volobujeva, in: J. Christen, C. Jagadish, D.C. Look, T. Yao, F. Bertram (Eds.), Zinc Oxide and Related Materials, Mater. Res. Soc. Symp. Proc., 957, 2007, Warrendale, PA 0957–K10-26.
[26] M. Altosaar, J. Raudoja, K. Timmo, M. Danilson, M. Grossberg, M. Krunks, T. Varema, E. Mellikov, Proceedings of the 2006 IEEE WCPEC-4, Havaii, 2006, May 7–12.
[27] K. Timmo, M. Altosaar, M. Kauk, J. Raudoja, E. Mellikov, Thin Solid Films 515 (2007) 5884.
[28] K. Tanaka, Y. Miyamoto, H. Uchiki, K. Nakazawa, H. Araki, Phys. Status. Solidi. (A) 203 (2006) 2891.
[29] J. Krustok, H. Collan, M. Yakushev, K. Hjelt, Phys. Scr. T79 (1999) 179.
[30] C.J. Brabec, N.S. Sariciftci, J.C. Hummelen, Adv. Funct. Mater. 11 (No 1) (2001) 15.
[31] A.J. Frank, S. Glenis, A.J. Nelson, J. Phys. Chem. 93 (1989) 3818.
[32] P. Chartier, H. Nguyen Cong, C. Sene, Sol. Energy Mater. Sol Cells 52 (1998) 413.

[33] Bereznev, J. Kois, I. Golovtsov, A. Öpik, E. Mellikov, Thin Solid Films 511–512 (2006) 425.
[34] S. Bereznev, R. Koeppe, I. Konovalov, J. Kois, S. Günes, A. Öpik, E. Mellikov, N.S. Sariciftci, Thin Solid Films 515 (2007) 5759.
[35] A. Verbitsky, Ya. Vertsimakha, P. Lutsyk, S. Studzinsky, S. Bereznev, J. Kois, Semiconductors 40 (Nr. 2) (2006) 197.
[36] M. Winkler, J. Griesche, I. Konovalov, J. Penndorf, J. Wienke, O. Tober, Sol. Energy 77 (2004) 705.
[37] Y. Roussillon, V.G. Karpov, Diana Shvydka, J. Drayton, A.D. Compaan, Proceedings of 31st IEEE Photovoltaic Specialists Conference, 2005, p. 441.